Diffusion Regularization for Iterative Reconstruction in Emission Tomography

Cyril Riddell, Habib Benali, and Irène Buvat

Abstract—We have recently proposed a regularized least square criterion for adaptive regularization of SPECT reconstruction with nonuniform attenuation correction. In the present study, we show that this regularization is closely related to a diffusion scheme used for Gaussian filtering. For a given value of the regularization parameter, the amount of smoothing is independent from the patient attenuation map, and it is mathematically related to the full width at half maximum (FWHM) of a Gaussian filter. A second regularized least square criterion is then derived for which regularization also behaves as a diffusion scheme. The new penalty is then shown to be also applicable to the weighted least square criterion, and to the Poisson maximum likelihood criterion for PET data (i.e., without attenuation) solved by the EM algorithm. For all these criteria, the regularization level can thus be set as the FWHM of a Gaussian filter.

Index Terms—Diffusion equations, least squares methods, OSEM, regularization, tomography.

I. INTRODUCTION

BECAUSE tomographic reconstruction is an ill-posed problem, regularization is necessary to control the noise propagation from the projections into the reconstructed images. For the regularization to be clinically practical, the resulting noise reduction and concomitant resolution loss should be *a priori* known. Unfortunately, with a patient-dependent modeling of the data, a given regularization parameter can produce smoothing effects that differ from patient to patient. A regularization penalty previously introduced in a least square adaptive regularization technique [1] is here demonstrated to behave as a diffusion scheme for Gaussian filtering. Resolution loss can therefore be set *a priori* as a full width at half maximum (FWHM). This regularization penalty is then extended to the weighted least square case and the OSEM algorithm for PET.

II. THEORY

A. Regularized Least Square Algorithm for SPECT

An image is estimated from a finite set of SPECT attenuated measurements by solving a linear system such as

$$R_a f = s_a \qquad (1)$$

where f is the unknown image vector, s_a is the attenuated SPECT sinogram, and R_a is a matrix that models SPECT tomographic acquisition with patient dependent nonuniform attenuation. A classical regularized least square solution of system (1) is given by minimizing

$$\min_f \{\|R_a f - s_a\|^2 + \alpha\|\nabla f\|^2\} \qquad (2a)$$

where α is a scalar and ∇f is the gradient of image f. This criterion is equivalent to solving

$$(R_a^t R_a + \alpha\Delta) f = R_a^t s_a \qquad (2b)$$

where ^{t} denotes the transpose of a matrix and Δ denotes the Laplacian operator.

When modeling attenuation, matrix R_a changes with the attenuation map, whereas the Laplacian is constant. Therefore, a fixed regularization value α generally yields a different smoothing for different patients.

B. Diffusion Regularization and Approximate Inversion

In a previous work [1], we have proposed to replace criterion (2) by the penalized frequency weighted least square [PFWLS] approach given by

$$\min_f \left\{ \left\|D_s^{1/2}(R_a f - s_a)\right\|^2 + \alpha\|\nabla\Gamma^{-1}f\|^2 \right\} \qquad (3a)$$

which is equivalent to solving

$$(T^t D_s T + \alpha\Delta)x = T^t D_s s_a \qquad (3b)$$

where $T = R_a\Gamma$, Γ represents the Chang correction, D_s stands for the ramp filtering operation in the sinogram domain, and x is such that $f = \Gamma x$. The ramp filter and Chang correction are used as a preliminary approximate inversion making the system matrix $T^t D_s T$ close to the identity matrix I, to speed convergence up and provide a normalization that allows for adaptive regularization with respect to noise [1].

In the present work, we further explore criterion (3) by considering that in (3b), $T^t D_s T$ differs from the identity for the effect of attenuation only. Attenuation is responsible for large biases with underestimation of the distribution values as large as 80% in cardiac SPECT, independently of the size of the structure [2]. Attenuation correction is thus required for quantification purpose rather than resolution recovery. We therefore hypothesize that attenuation mainly affects the low frequency content

of an image so that the regularization constraint in (3b) will produce the same filtering as in the absence of attenuation, i.e., as in the following diffusion scheme:

$$(I + \alpha\Delta)f = f_0 \tag{4}$$

where f_0 is the image to be filtered. The solution f of system (4) tends toward f_0 filtered by a Gaussian kernel with FWHM equal to $3.33\sqrt{\alpha}$ [3]. We therefore define the regularization penalty in (3) as a diffusion regularization.

An alternative approximate inversion of (1) is obtained by applying the ramp filter in the image domain [4], giving

$$(D_i T^t T + \alpha\Delta)x = D_i T^t s_a \tag{5}$$

where D_i stands for the ramp filtering operation in the image domain. Again, system (5) differs from the diffusion scheme (4) by the effect of attenuation only. Under the same hypothesis that attenuation mainly affects the low frequency content of an image, we expect that the Laplacian term will produce a diffusion filtering. Moreover, using the relation $\Delta x = (D_i)^2 x$, system (5) can be simplified into

$$(T^t T + \alpha D_i)x = T^t s_a \tag{6a}$$

which leads to the following penalized least square [PLS] criterion:

$$\min_f \left\{ \|R_a f - s_a\|^2 + \alpha \left\| D_i^{1/2} \Gamma^{-1} f \right\|^2 \right\} \tag{6b}$$

where $D_i^{1/2}$ stands for the filtering of an image by the square root of the ramp filter.

Criterion (6) is equivalent to (3) in the absence of attenuation and since we assume that attenuation mainly affects the lower frequencies of the image, we do not expect significant differences in the regularization output of criteria (3) and (6). The interesting finding is that the regularization in (6), that is based on ramp filtering, allows for extending diffusion regularization to criteria that are not derived from a prior approximate inversion of the system matrix. This was not the case with the Laplacian based regularization of (3) that behaves as a diffusion regularization because of the prior approximate inversion of the system.

C. Diffusion Regularization for the Weighted Least Square Case and the OSEM Algorithm

For the sake of simplicity, we describe the weighted least square criterion for the nonattenuated case only. It is expressed as

$$\min_f \|\Sigma^{-1/2}(Rf - s)\|^2 \tag{7}$$

where Σ is a diagonal matrix with each diagonal term equal to the inverse weight of the corresponding measurement (e.g., its variance). Matrix R and vector s respectively replace matrix R_a and vector s_a in the nonattenuated case. The introduction of the variance of the measurements makes the criterion dependent upon each specific patient data set. Adding a regularization constraint with fixed strength will therefore not yield uniform resolution over the reconstructed image, neither the same filtering

effect from one patient to the other [5]. For constant weights Σ, diffusion regularization is obtained with the ramp filter penalty given in (6). Independence from the weights is obtained by applying a normalization term through a diagonal operator P such as the one given in [5], which yields the following regularized criterion:

$$\min_f \left\{ \|\Sigma^{-1/2}(Rf - s)\|^2 + \alpha \left\| D_i^{1/2} P^{-1} f \right\|^2 \right\} \tag{8a}$$

equivalent to solving

$$(P R^t \Sigma^{-1} R P + \alpha D_i)y = P R^t \Sigma^{-1} s \tag{8b}$$

where y is such that $f = Py$.

If the data variance estimates are set equal to the data mean estimates, the criterion is similar to maximizing a Poisson likelihood. This suggests that applying the same penalty based on ramp filtering to the EM algorithm should provide equivalent diffusion regularization. In this study, the penalty was implemented with the one-step-late method combined to the ordered subset acceleration technique [6]. The penalty term was computed at each subiteration, and the normalization matrix P was computed for each subset as a simple backprojection over the subset of the measurement weights.

In the case of attenuation, the Chang correction Γ can be multiplied to the P matrix for normalizing the weighted least square criterion for SPECT [5]. With OSEM, this is not possible because the algorithm formula already contains a normalization term that includes attenuation. A separate analysis is therefore required as a future work. Diffusion regularization as given by the penalty of (8a) was therefore applied with OSEM to nonattenuated emission data (such as attenuation pre-corrected PET data) in this work.

D. Class-Dependent Diffusion Regularization

When diffusion regularization is applied with the Laplacian operator, it offers the additional possibility of selectively smoothing the reconstructed image by regions. Here, the regions are supposed to be defined *a priori*, for instance as classes resulting from the segmentation of the attenuation map, which keeps the problem linear. The Laplacian operator, scaled by α, can be implemented as the four-point spatial kernel that is, at pixel k, the sum of each difference of pixel k minus its neighbors, weighted by α. A simple modification of this sum allows for a class-dependent filtering: each difference between two neighboring pixels k and l is weighted with a different "local" α, denoted α_{kl}, which determines the local level of smoothing. By setting $\alpha_{kl} = \alpha_{lk}$, the system is kept symmetric. This level is held constant for all differences between pixels belonging to the same class, but can change from class to class. For a given class, it is denoted α (class). In addition, a level of smoothing is defined between all classes that is denoted $\bar{\alpha}$. When pixels k and l belong to the same class, α_{kl} is set to α (class), otherwise it is set to $\bar{\alpha}$. The values of α (class) and $\bar{\alpha}$ are related to FWHM values by the same relation $3.33\sqrt{\alpha(\text{class})}$ and $3.33\sqrt{\bar{\alpha}}$.
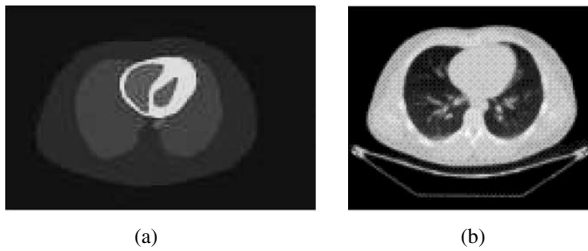
Fig. 1. (a) Simulated cardiac emission distribution and (b) CT attenuation map from the Zubal phantom.

III. EXPERIMENTS

Effectiveness of diffusion regularization was examined through simulation of attenuated SPECT data in the case of the least square criteria and nonattenuated data in the case of the OSEM algorithm.

A segmented CT slice at the heart level of the Zubal phantom [7] was considered. Activity was simulated by setting the cardiac muscle region to 10, the blood pool region to 3, and the lung region to 2, while all other tissues were set to 1 [Fig. 1(a)]. This activity distribution is called "reference image" in the following.

Three sets of projections of the reference image (120 projections over $360°$, 128 measurement bins, parallel geometry) were obtained, corresponding to three different attenuation maps. The first set corresponded to the no attenuation case ($\mu = 0$), the second, called "Tc-99m" data, corresponded to the CT attenuation map [Fig. 1(b)] scaled to 140 keV, and the third, called "Tl-201", corresponded to the CT attenuation map scaled to 70 keV. Using Poisson noise simulations, 40 replicate noisy sinograms were computed for each data set. The total number of counts per sinogram was about 1 000 000 for the nonattenuated data, 270 000 for the Tc-99m data and 200 000 for the Tl-201 data.

All attenuated projection sets were reconstructed (128×128 grid, pixel size 4 mm) with the conjugate gradient algorithm to solve the PFWLS criterion defined by (3) and the PLS criterion defined by (6) with 15 iterations in each case. All nonattenuated data sets were reconstructed with the OSEM algorithm with 10 iterations and 10 subsets. For all algorithms, the regularization parameter was varied between 2 and 6 pixels when expressed as FWHMs, corresponding to α values ranging from 0.36 to 3.25. Convergence of the reconstruction algorithms was monitored by computing the root mean square error (RMSE) between the images obtained at each iteration and the reference image. Diffusion regularization was compared to the direct filtering of the reference image with the diffusion scheme derived from (4) that is described in [3] using the same values for α. Resolution was assessed by comparing such filtering to the average of the replicate regularized reconstructions which were virtually noise free. For OSEM, robustness of the regularization output with respect to the amount of noise was also tested by simulating a high noise level corresponding to an acquisition of ten times less counts (i.e., 100 000 counts per sinogram).

Five impulses (defined as one voxel set to 0.1) sampling both lungs, the heart, and the surrounding tissues, were also projected and added to the replicate data sets. Reconstruction of the impulses was obtained by subtracting the average reconstruction
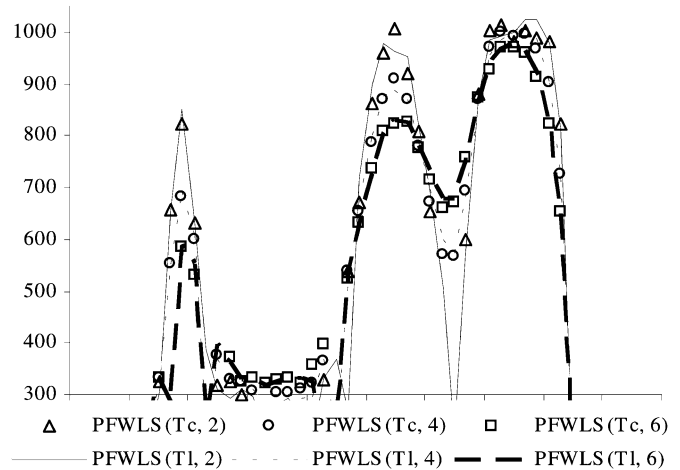

Fig. 2. Horizontal profiles through PFWLS average reconstruction for Tc-99m data with FWHM values of 2 (triangles), 4 (circles) and 6 (squares) pixels compared to the PFWLS average reconstruction for Tl-201 data with the same FWHM values of 2 (solid line), 4 (dashed line), and 6 (bold dashed line) pixels.

of the impulse-free data from the average reconstruction of the data containing the added impulses. Due to the interpolation of the projection step, the impulses were smoothed in the data and their reconstruction did not correspond to the impulse response of the regularization, but it allowed for analyzing the stationarity of this response.

Class-dependent regularization was applied to one Tc-99m noisy data set, to demonstrate class-dependent noise reduction. The CT attenuation map was segmented into three classes: bone and soft tissues (i.e., including blood pool and myocardium), lungs, and background (outside of the body). Four FWHM values were used: 2 pixels for the soft tissues, 4 pixels for the lungs, 6 pixels for the background, and 4 pixels between classes. Selective noise reduction was assessed by considering the difference between the reconstructed image and the images reconstructed with PFWLS and uniform regularization with FWHM values of 2, 4, and 6 pixels.

IV. RESULTS

Convergence of the PFWLS algorithm was monitored when reconstructing noise free Tc-99m data and Tl-201 data with α set to 0.81. With a normalized $T = R_a \Gamma$ in (3b), the ratio between the patient-dependent model and the regularization term was kept constant enough from one attenuation map to the other to maintain the same regularization bias in each case (final RMSE of 0.197 for the Tc-99m data and 0.198 for the Tl-201 data). This was not true without normalization ($T = R_a$ in (3b), with α set to 0.05). In that case, the matrix describing the highest attenuation had the smallest norm yielding the highest bias and smoothing (final RMSE of 0.225 for the Tc-99m data versus 0.268 for the Tl-201 data). On Fig. 2, profiles at the heart level through the average of the replicate PFWLS reconstructions show the amount of filtering that was obtained with the Tc-99m data and regularization with FWHM values of 2 (triangles), 4 (circles), and 6 (squares) pixels, and with the Tl-201 data with the same FWHM values (lines). A very good overlap of the symbols over the corresponding lines
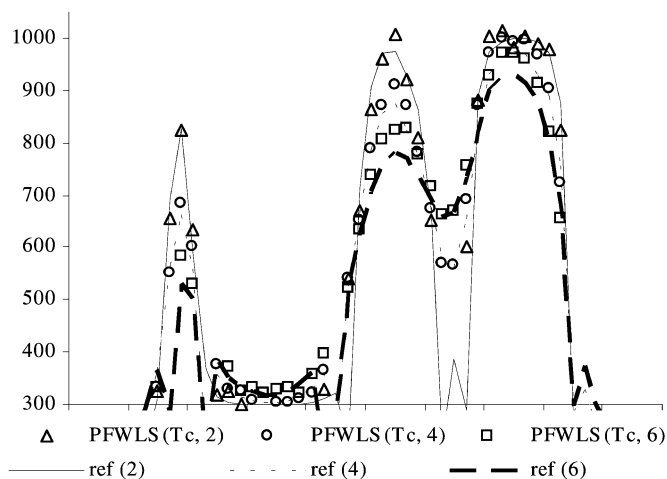
Fig. 3. Horizontal profiles through PFWLS average reconstruction for Tc-99m data with FWHM values of 2 (triangles), 4 (circles), and 6 (squares) compared to the reference image filtered with the same FWHM values of 2 (solid line), 4 (dashed line), and 6 (bold dashed line) pixels.
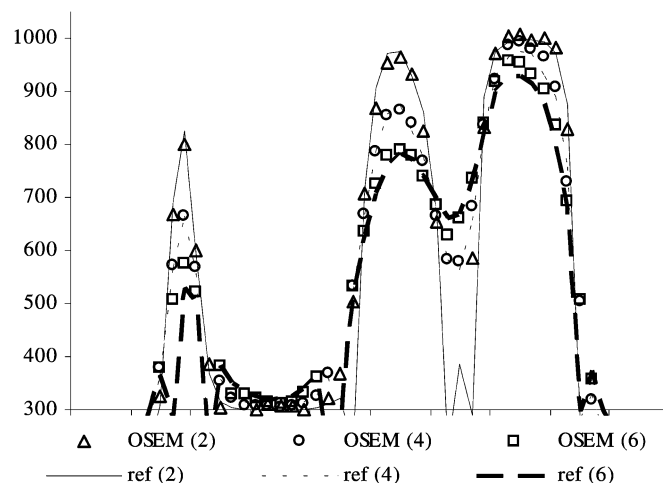

Fig. 4. Horizontal profiles through OSEM average reconstruction with FWHM values of 2 (triangles), 4 (circles), and 6 (squares) compared to the reference image filtered with the same FWHM values of 2 (solid line), 4 (dashed line) and 6 (bold dashed line) pixels.

was obtained for the three levels of regularization. Diffusion regularization was therefore independent from the attenuation map, and from the noise level since the more attenuated Tl-201 data had more noise.

Fig. 3 compares the same profiles of Fig. 2 obtained with PFWLS and the Tc-99m data, to diffusion filtering of the reference image. A very good agreement is seen for a 2-pixel regularization (triangles for PFWLS and solid line for diffusion filtering). However, as the regularization level increased to 4 (circles) and 6 (squares) pixels, the regularization constraint produced less smoothing than the diffusion scheme (dashed lines).

Fig. 4 compares the profiles at the same level of the heart through the average of the replicate OSEM reconstructions (symbols) to the same profiles through the reference image filtered with the diffusion scheme (lines) as in Fig. 3. The agreement between the regularization and the diffusion filter is shown by a good overlap of the symbols over the corresponding lines. However, for an FWHM value of 6 pixels (squares versus bold dashed line), the smallest peak on the left was less smoothed by the regularized OSEM than by the diffusion filter. The results obtained from averaging replicate reconstructions with ten times more noise were identical (profiles not shown).

Fig. 5 top image shows the impulse locations over the attenuation map (impulses were one pixel wide). Horizontal profiles were taken through each impulse. The plot of Fig. 5 shows these profiles in the case of the PFWLS reconstruction of Tc-99m data with FWHM of 2, 4, and 6 pixels. For each FWHM value, the profiles of the five impulses have been concatenated. The plot shows that filtering was not perfectly uniform: for attenuated data, the amount of filtering was inversely proportional to the distance to the center. Considering the standard deviation of the peak values of the five impulses, the variation was 8.3% (resp.: 8.7% and 9.2%) of the average peak value for an FWHM of 2 (resp.: 4 and 6) pixels. The same dependency was observed with the Tl-201 data. With OSEM, this variation was 13.5% (resp.: 10.4% and 12.3%) for the same FWHM of 2 (resp.: 4 and 6) pixels, but it did not show any radial pattern (profiles not shown).
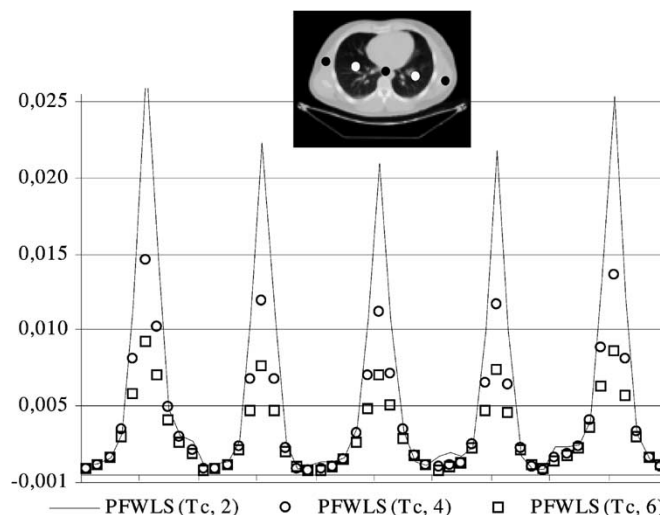

Fig. 5. Concatenated horizontal profiles of five small impulses obtained from PFWLS reconstructions of Tc-99m data with FWHM values of 2 (solid line), 4 (circles), and 6 (squares) pixels. (The center of the black and white circles added to the attenuation map indicate the locations of the impulses.)

Fig. 6 allows for a direct comparison of the averages of the replicate reconstructions according to the data set, the algorithm, and the regularization level. The columns correspond to OSEM, PFWLS with Tc-99m data, PLS with Tc-99m data, and PFWLS with Tl-201 data. Each row shows a different level of regularization, from row A with no regularization (0) to row D that corresponds to a diffusion regularization with an FWHM of 6 pixels. In spite of the variations in the noise level (the noise increased with attenuation), the attenuation maps, and the reconstruction algorithms, differences in the regularization output are not visible on row B, i.e., for an FWHM value of 2 pixels. As the FWHM increased (rows C and D), images produced by diffusion regularization with PFWLS were, as already shown on Fig. 2, independent from the attenuation map, but slightly less smoothed than OSEM, whereas PLS images were noticeably less smoothed. PLS results were also independent from the attenuation map (Tl-201 images not shown).
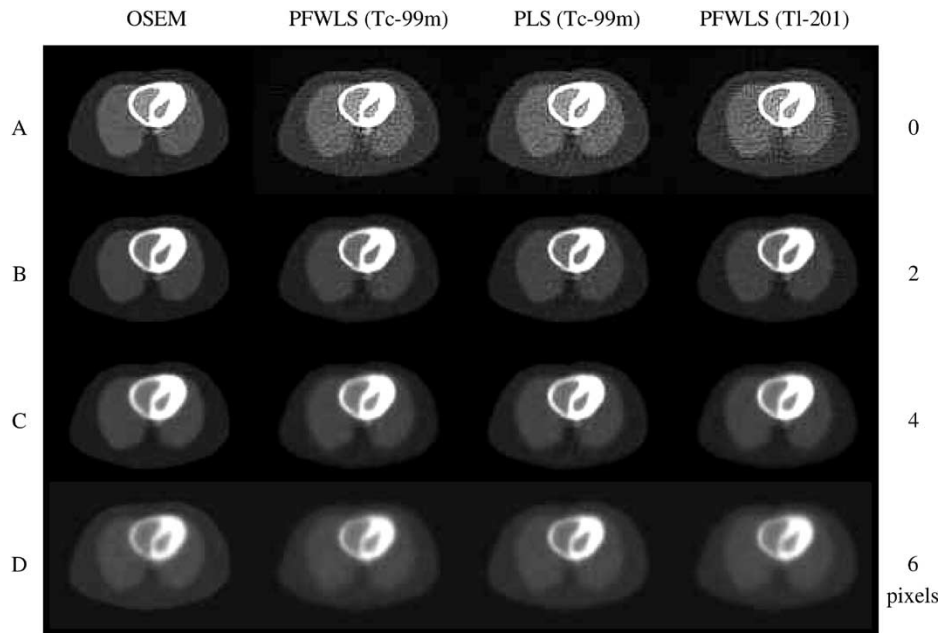
Fig. 6.   Average reconstruction for OSEM (1st column), PFWLS (2nd column for Tc-99m data and 4th column for Tl-201 data) and PLS (3rd column) according to the level of regularization (FWHM values from 0 to 6 pixels).
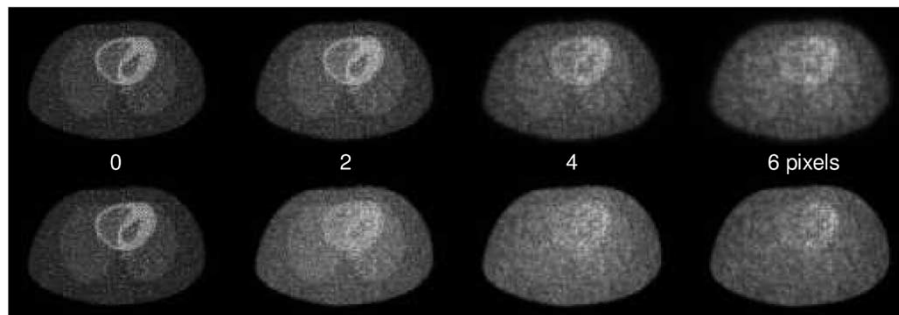

Fig. 7.   Standard deviation images computed from reconstruction of high noise replicate nonattenuated data (images are scaled to their own maximum). Top row: nonregularized OSEM reconstruction has been post-filtered by a diffusion filter with FWHM values of 0 to 6 pixels. Bottom row: diffusion regularized OSEM reconstruction with the same FWHM values.

Fig. 7 compares the noise properties of the OSEM reconstruction with regularization and without regularization but diffusion post-filtering. The images show the standard deviation at each pixel computed from the 40 replicate reconstructions. Without regularization nor post-filtering (left column, the same image is shown twice) the standard deviation of the noise at a given pixel is proportional to the mean intensity of that same pixel, as expected with OSEM [8]. With diffusion post-filtering, the standard deviation is more and more uniform as the FWHM increases (top row). Using diffusion regularization, the standard deviation also becomes more uniform, but at a faster pace than with post-filtering (bottom row). Note that, as shown on the profiles of Fig. 4, the comparison is made at matched resolution for a small FWHM value, whereas for higher values, the use of the diffusion regularization yielded slightly less smoothing than post-filtering. Still, regularized reconstructions led to the most uniform noise images. For an FWHM value of 2 pixels, the standard deviation was on average 25% greater in the myocardium with diffusion post-filtering. There was no significant difference in the lungs and the cavity, whereas the noise was on average 18% higher in the external tissues with diffusion regularization.

Fig. 8 shows the PFWLS reconstruction of noisy data with a region-dependent regularization of FWHM values of 6 pixels in the background outside of the body, 4 pixels in the lungs, and 2 pixels in all other tissues (left image, inverse grey scale). Images A, B, C are the difference images between the region-dependent regularization and the PFWLS reconstructions with uniform regularization of FWHM value of 2 (image A), 4 (image B), and 6 (image C) pixels. Image A (resp.: B and C) shows that the region-dependent regularization had the same smoothing effect over the tissues (resp.: lungs and background) than a uniform 2-pixel (resp.: 4-pixel and 6-pixel) regularization, as expected. Therefore the PFWLS algorithm regularized with the modified Laplacian operator allows for a modulated noise reduction according to *a priori* defined regions.

V. DISCUSSION

Iterative reconstruction algorithms are used to correct for nonuniform attenuation in SPECT or improve the noise
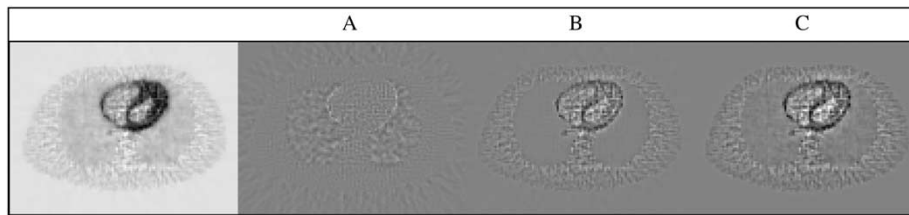
Fig. 8.   Left image: PFWLS reconstruction of noisy data with a region-dependent regularization with FWHMs of 6 pixels outside of the body, 4 pixels in the lungs, and 2 pixels in all other tissues. Images A, B, C: difference images with PFWLS reconstructions with uniform regularization and FWHM of 2 (A), 4 (B), and 6 (C) pixels.

properties of low-count PET data. In order to control the noise increase inherent to tomographic reconstruction of noisy data, regularization is applied. However, setting the proper regularization parameter has proved difficult in clinical routine, due to the fact that a given regularization weight produces different smoothing levels according to the patient dependent model [5]. In the present work, we have proposed three reconstruction criteria whose regularization output was not dependent upon the patient attenuation map or data weighting for reasonable amounts of regularization. For the OSEM algorithm and two penalized least square criteria, that all produce regularized images based on patient dependent models, it was possible to interpret the regularization constraint as a diffusion scheme independent from the attenuation map or variance estimates, and to relate the regularization parameter to the FWHM of a Gaussian filter. For a smoothing level of 2 pixels, the proposed regularization produced the same smoothing effect as the diffusion scheme independently of the attenuation map, the noise level, and the statistical criterion.

In the presence of attenuation, the PFWLS and PLS algorithms showed less-than-expected filtering for FWHM values of 4 and 6 pixels, suggesting an increasing interference between attenuation and regularization. The reason why this interference affected PLS more than PFWLS will require further investigation. This interaction also affected the uniformity of the filtering, with a slightly sharper response away from the center of the image.

In the case of OSEM, diffusion regularization and diffusion filtering resulted in a very similar resolution loss, with still a slightly less-than-expected filtering at 6 pixels when using the regularization, and slight nonstationarity. Both diffusion regularization and diffusion post-filtering lead to uniform standard deviation images as the FWHM increased, removing the proportionality between the level of noise and the level of intensity at a given pixel of a reconstructed image, a specificity of the OSEM algorithm [8]. However, this removal happened at a faster pace with diffusion regularization than with diffusion post-filtering. One must therefore be careful when using OSEM and diffusion regularization, that one is not losing the specific noise properties that called for the use of OSEM in the first place, as in oncology where OSEM ability to avoid noise spread of the image can be an advantage over analytical reconstruction [9]. Similar results have been obtained in [10] where the authors derived filters that matched common regularization penalties tuned to produce uniform and patient independent output. Contrary to our study, these filters were different from common filters such as Gaussian diffusion, but the authors also concluded that regular-

ization yielded noise characteristics that were different from that of the corresponding post-filtering.

Since a 2-pixel diffusion filtering is very close to using the Hamming filter with cut-off frequency 0.5 of standard filtered backprojection, this regularization value could be applied in all cases, ensuring and speeding convergence to an image with a well characterized filtering, while preserving the noise properties enforced by the statistical criterion. To compensate for increased noise from one patient to the other, further filtering could be applied *after* reconstruction with (faster) digital filters.

Further work is needed to combine diffusion regularization with OSEM in the presence of attenuation, as the question of the normalization is not a direct extension of the least square case any more. Diffusion regularization remains compatible with the weighted least square criterion, which is a valid approach to reconstructing attenuated SPECT data affected by Poisson noise [11].

The adaptive procedure proposed in [1] is an alternative solution for noise removal in the clinical setting that is even more attractive now that we have a characterization of the filtering and an interpretation of the regularization value delivered by the algorithm in terms of resolution.

Finally, region-dependent diffusion regularization based on anatomical information was also demonstrated in the framework of least square reconstruction. In such a case, high regularization values were used in background areas where precise prediction of the filtering effect was not as important, allowing for the "cleaning" of the image.

VI. CONCLUSION

We have proposed two regularization penalties adapted to either the least square, the weighted least square or the OSEM algorithm that provide the same filtering effect as a diffusion scheme used for Gaussian filtering. Diffusion regularization is independent from the patient model and the regularization parameter is mathematically linked to the FWHM of a Gaussian filter, making the level of smoothing induced by regularization easy to control.

REFERENCES

[1] C. Riddell, I. Buvat, A. Savi, M. C. Gilardi, and F. Fazio, "Iterative reconstruction of SPECT data with adaptive regularization," *IEEE Trans. Nucl. Sci.*, vol. 49, pp. 2350–2354, 2002.

[2] G. N. El Fakhri, I. Buvat, M. Pélégrini, H. Benali, P. Almeida, B. Bendriem, A. Todd-Pokropek, and R. Di Paola, "Respective roles of scatter, attenuation, depth-dependent collimator response and finite spatial resolution in cardiac single-photon emission tomography quantitation: A Monte Carlo study," *Eur. J. Nucl. Med.*, vol. 26, pp. 437–446, 1999.

[3] J. Weickert, B. M. ter Haar Romeny, and M. A. Viergever, "Efficient and reliable schemes for nonlinear diffusion filtering," *IEEE Trans. Image Processing*, vol. 7, pp. 398–410, 1998.

[4] N. H. Clinthorne, T. S. Pan, P. C. Chiao, W. L. Rogers, and J. A. Stamos, "Pre-conditioning methods for improved convergence rate in iterative reconstruction," *IEEE Trans. Med. Imaging*, vol. 12, pp. 78–83, 1993.

[5] J. A. Fessler and W. L. Rogers, "Spatial resolution properties of penalized-likelihood image reconstruction: Space-invariant tomographs," *IEEE Trans. Image Processing*, vol. 5, pp. 1346–1358, 1996.

[6] H. M. Hudson and R. S. Larkin, "Accelerated image reconstruction using ordered subsets of projection data," *IEEE Trans. Med. Imaging*, vol. 13, pp. 601–609, 1994.

[7] I. G. Zubal, C. R. Harrell, and E. Smith, "Computerized 3D segmented human anatomy," *Med. Phys.*, vol. 21, pp. 299–302, 1994.

[8] H. H. Barrett, D. W. Wilson, and B. M. W. Tsui, "Noise properties of the EM algorithm: I. Theory," *Phys. Med. Biol.*, vol. 39, pp. 833–846, 1994.

[9] C. Riddell, R. E. Carson, J. A. Carrasquillo, S. K. Libutti, D. N. Danforth, M. Whatley, and S. L. Bacharach, "Noise reduction in oncology FDG PET images by iterative reconstruction: A quantitative assessment," *J. Nucl. Med.*, vol. 42, pp. 1316–1323, 2001.

[10] J. Nuyts and J. A. Fessler, "A penalized-likelihood image reconstruction method for emission tomography, compared to post-smoothed maximum-likelihood with matched spatial resolution," *IEEE Trans. Med. Imaging*, vol. 22, pp. 1042–1052, 2003.

[11] E. P. Ficaro, J. A. Fessler, R. J. Ackerman, W. L. Rogers, J. R. Corbett, and M. Schwaiger, "Simultaneous transmission-emission Thallium-201 cardiac SPECT: Effect of attenuation correction on myocardial tracer distribution," *J. Nucl. Med.*, vol. 36, pp. 921–931, 1995.